

## Effects of Large-Angle Coulomb Collisions on Inertial Confinement Fusion Plasmas

A. E. Turrell,<sup>\*</sup> M. Sherlock, and S. J. Rose

*Imperial College London, South Kensington SW7 2AZ, United Kingdom*

(Received 4 December 2013; published 20 June 2014)

Large-angle Coulomb collisions affect the rates of energy and momentum exchange in a plasma, and it is expected that their effects will be important in many plasmas of current research interest, including in inertial confinement fusion. Their inclusion is a long-standing problem, and the first fully self-consistent method for calculating their effects is presented. This method is applied to “burn” in the hot fuel in inertial confinement fusion capsules and finds that the yield increases due to an increase in the rate of temperature equilibration between electrons and ions which is not predicted by small-angle collision theories. The equilibration rate increases are 50%–100% for number densities of  $10^{30} \text{ m}^{-3}$  and temperatures around 1 keV.

DOI: [10.1103/PhysRevLett.112.245002](https://doi.org/10.1103/PhysRevLett.112.245002)

PACS numbers: 52.25.Fi, 52.57.–z, 52.65.Pp

Large-angle Coulomb collisions could affect the collision rates of exchange of energy in plasmas relevant to inertial confinement fusion (ICF) [1–3], even for the simplest initial conditions of the hot fuel spot, or “hot spot,” at the center of an ICF capsule. The rates of energy exchange influence the hot spot yield, which then determines whether a burn wave will be initiated.

An igniting ICF hot spot will have conditions [4] of areal density and temperature of  $\sim 0.3 \text{ g/cm}^2$  and  $\sim 10 \text{ keV}$ , respectively. For the expected hot spot radius of tens of microns, these conditions correspond to small values of the Coulomb logarithm  $\ln \Lambda$ . It is well known that the relative importance of large-angle Coulomb collisions to the small-angle Coulomb collisions which dominate interactions in classical plasmas is  $\mathcal{O}(1/\ln \Lambda)$  [5]. There is currently no self-consistent method for calculating the effects of large-angle Coulomb collisions in plasmas, and their inclusion is a long-standing problem [5–7].

Calculating their effects is therefore expected to be important in the  $2 \lesssim \ln \Lambda \lesssim 5$  regime, which includes high intensity laser-plasma interactions at solid density [8], degenerate plasmas [9], ICF, and stellar cores [10,11]. Wide ranging experimentally detectable consequences of large-angle collisions have been described for the shape and evolution of distribution functions [12–15], for fusion reactivities or as a diagnostic in both ICF and magnetic confinement fusion [16–23], for plasma properties such as particle stopping and temperature equilibration [24–26], and for “athermal” fusion [3,27]. The first experimental observation of a non-Maxwellian distribution due to large-angle collisions was on the JET tokamak [28].

We have, for the first time, developed a way of performing fully self-consistent calculations of the effects of large-angle collisions that apply to plasmas with  $\ln \Lambda \gtrsim 2$ . In this Letter, we present this method, demonstrate its use, and show that there are significant differences with small-angle collision only theories.

The most dramatic effect is to increase the yield beyond what is predicted by small-angle-only theories by 20%–70% in 6 ps depending on the choice of large-angle collision model when considering the evolution of a simple hot spot. This increase occurs because large-angle collisions allow the reacting ion species, deuterium (D) and tritium (T), to heat up more quickly than when only counting small-angle collisions, and the neutron yield in ICF is strongly dependent on ion temperature. The attainment of higher temperatures earlier is due to an increase in the rate of equilibration of temperature between ions and electrons [29]. This is a direct consequence of the self-consistent inclusion of large-angle collisions.

Large-angle collisions involve a large transfer of energy or momentum per collision, as opposed to small-angle collisions. These two types of collision are also known as “close” and “remote” collisions, respectively, due to the relationship between impact parameter  $b$  and scattering angle  $\theta$  of  $b = b_{\perp} \cot(\theta/2)$ . Here,  $b_{\perp} = (q_i q_j / 4\pi\epsilon_0) (1/m_{ij} v_{ij}^2)$ , and  $q$  is the charge,  $m_{ij}$  is the reduced mass,  $v_{ij}$  is the relative velocity, and the species are denoted by  $i$  and  $j$ .

Other plasma theories, such as Vlasov-Fokker-Planck (VFP), are only applicable in classical plasmas with  $\ln \Lambda \gg 1$  as they either ignore large-angle Coulomb collisions [15], approximate them by overcounting the effects of small-angle collisions in  $\ln \Lambda$  [6], or have to be expanded to higher order in the change in momentum in a collision to recover some of the effects [25].

Though small-angle collisions are important for the overall exchange of energy in plasmas with  $2 \lesssim \ln \Lambda \lesssim 5$ ,

---

*Published by the American Physical Society under the terms of the Creative Commons Attribution 3.0 License. Further distribution of this work must maintain attribution to the author(s) and the published article's title, journal citation, and DOI.*

the impact of fewer large-angle collisions with larger transfers of energy per collision cannot be ignored; they must be taken into account in order to get the rate of exchange of energy correct [25,26]. That the changes in energy per collision are discontinuous is also important; continuous loss models fail for large-angle scattering [30].

Existing models of large-angle collisions are not self-consistent. Some only model the athermal part of the distribution function, and neglect feedback on its bulk [3], or assume a steady state [27]. Others use an initial non-Maxwellian distribution, but evolve it using the small-angle-only VFP equation [19]. A cutoff in impact parameter is always required, and is either  $\sim b_\perp$  or is imposed by computational limits. We develop an approximate theory for the cutoff based on physical motivations.

We take large-angle collisions to be true binary collisions, where the full postcollision trajectory is followed according to the Rutherford cross section. This is different from “multiple” small-angle scattering in which a particle is deflected due to an ensemble of particles within its Debye sphere (a sphere of radius the plasma Debye length  $\lambda_D$ ). Multiple small-angle scattering is described using the binary collision approximation, but particles undergoing this scattering do not follow the postcollision trajectory of two particles interacting with the Rutherford cross section. There are two equivalent pictures of the origin of large-angle, and multiple small-angle, collisions.

In one, described by Cohen, Spitzer, and McRoutly [6], and others [5,31], it is the long range of the Coulomb force that causes remote particles to dominate interactions in classical plasmas. These long-range forces are cut off at  $b = \lambda_D$  in order to avoid the divergence in the cross section. However, they note that there must be some finite distance  $b_c \leq \lambda_D$  where the interaction with one other particle becomes dominant, that if there were no large deflections, then plasmas would be fully described by VFP, and that the omission of large-angle encounters introduces a larger error as  $\lambda_D/b_\perp$  and  $\ln \Lambda$  become smaller. The other view, from Sivukhin [7], is that the divergence arises because Rutherford implicitly assumes infinite interaction times, but the time for remote interactions must be constrained. This is because deflection angles in remote collisions must both be small and increase with interaction time. Large-angle collisions are effectively instantaneous by comparison; thus, particles follow the “full” Rutherford collision trajectory.

All of the authors recommend approximating large-angle collisions by using  $b_c = 0$ , with Sivukhin adding, “Such an approach ... cannot pretend to give a completely adequate description of the true situation.” Both interpretations suggest the use of an impact parameter  $b = b_c$  that defines the crossover between large- and small-angle scattering, so that the former is restricted in angle to  $|\theta_c(b_c)| \leq |\theta| \leq \pi$  and the latter to  $0 \leq |\theta| < |\theta_c(b_c)|$ .

Values for  $b_c$  used by previous authors include 0,  $b_\perp$ ,  $2b_\perp$  [5],  $5.67b_\perp$  [19], and values set by computational considerations [3]. Following other authors, simulations are performed with  $b_c = b_\perp$ , which corresponds to a cutoff in angle of  $\theta_c = \pi/2$ , and  $b_c = 0$ , which corresponds to Monte Carlo calculations with small-angle collisions only. Additionally, it is desirable to perform calculations with a physically motivated cutoff, and one approach would be to use molecular dynamics (MD) simulations. However, MD interactions are typically cut off at short range (to prevent electrons becoming infinitely bound) with an arbitrary “smoothing parameter” or “small-ball radius” [32], and  $b_c$  would be sensitive to this parameter.

We therefore perform calculations with a third, physically motivated, value of  $b_c$  based on determining the distance at which the potential on particle  $i$  due to particle  $j$  is larger than the potential at  $i$  due to *all* other particles. We define this cutoff as  $b_c = b_\phi$ . Calculating  $b_\phi$  requires an assumption about the potential; a Yukawa potential, screened by  $\lambda_D$ , is a good model even for strongly coupled plasmas with  $N_D \sim 1$  [33,34], where  $N_D$  is the number of particles in a Debye sphere. Let  $i$ ,  $j$ , and  $m$  represent particles. The potential at  $i$  due to  $j$  is  $\phi_{ji}(\mathbf{r}_{ij}) = q_j e^{-r_{ij}/\lambda_D} / (4\pi\epsilon_0 r_{ij})$ , where  $r_{ij}$  is the distance of  $j$  from  $i$ . For  $i$ ,  $b_\phi$  is the value of  $r_{ij}$  which satisfies

$$\phi_{ji}(\mathbf{r}_{ij}) = \sum_{m \neq i,j} \phi_{mi}(\mathbf{r}_{im}), \quad (1)$$

where  $j$  is the nearest neighbor (of its species) of  $i$ , and  $m$  runs over *all* other particles. Substituting  $r_{ij} = b_\phi(j, i)$  in Eq. (1) gives  $\phi_{ji}(b_\phi) = \sum_m \phi_{mi}(r_{im})$ . Evaluating  $r_m$  time dependently would mean solving Liouville’s equation, so an average model is used. Let  $s$  represent a species. It is assumed that the distance to the nearest particle of species  $s$  will be, on average, found from  $\frac{4}{3}\pi r_s^3 n_s = 1$ . Let  $r_s \equiv r_{s:1} = (4\pi n_s/3)^{-1/3}$ , then the  $m$ th particle away is given by  $r_{s:m} = m^{1/3} r_s$ . That average particle separations are  $\propto r_0$  is supported by the Holtsmark theory [35,36]. Then  $\phi_{ji}(b_\phi) = \sum_s q_s I_s / (4\pi\epsilon_0 r_s)$ , where

$$I_s \approx \frac{3}{x} e^{-k^{1/3}x} \left( k^{1/3} + \frac{1}{x} \right) + \sum_{m=0}^k \frac{e^{-m^{1/3}x}}{m^{1/3}}, \quad (2)$$

where  $x = r_s/\lambda_D$ ,  $s$  is species,  $m$  runs over all particles of species  $s$ , and it is assumed that the  $m \rightarrow \infty$  limit can be taken. Equation (1) is solved numerically with  $k \gtrsim 50$  to ensure convergence. When two species have different charges, the lower of the two values of  $b_\phi$  is used to ensure both experience a true binary collision. Using  $b_c = b_\phi$ , the probability of large-angle collisions relative to small-angle collisions tends to zero for large  $\ln \Lambda$ .

A plasma Monte Carlo code [37,38] has been extended to include large-angle collisions with a cutoff at  $b_c$ . The code includes fusion of D and T ions, a feature that

has been benchmarked against other results [39]. In multiple-scattering-only Monte Carlo calculations, angles are picked from  $\theta \sim \mathcal{N}(0, \langle \Theta^2 \rangle)$ , where  $\langle \Theta^2 \rangle = n \Delta t v_{ij} 8\pi b_{\perp}^2 \ln \Lambda$ .  $\Delta t$  is the computational time step, and  $n = \min\{n_i, n_j\}$ . The modified collision algorithm requires that multiple scattering be restricted to impact parameters  $b \in (b_c, b_{\max})$  and a variance of  $\langle \Theta^2 \rangle = n v_{ij} \Delta t 8\pi b_{\perp}^2 \ln \Lambda_M$ , where

$$\ln \Lambda_M = \frac{1}{2} \ln \left( \frac{b_{\min}^2 + b_{\max}^2}{b_{\min}^2 + b_c^2} \right), \quad (3)$$

$$\ln \Lambda_L = \frac{1}{2} \ln \left( \frac{b_{\min}^2 + b_c^2}{b_{\min}^2} \right), \quad (4)$$

and the total Coulomb logarithm is  $\ln \Lambda_M + \ln \Lambda_L = \ln \Lambda$ . Subscripts  $M$  and  $L$  refer to multiple and large-angle scattering, respectively. Also,

$$b_{\max}^2 \equiv \lambda_D^2 + r_0^2; \quad b_{\min}^2 \equiv \lambda_{\text{dB}}^2 + b_{\perp}^2, \quad (5)$$

where the total particle sphere radius is  $r_0 = (4\pi \sum_i n_i/3)^{-1/3}$ , and  $\lambda_{\text{dB}}$  is the de Broglie wavelength. Subsequent references to  $\ln \Lambda$  mean this version, which is valid for  $N_D \gtrsim 10$  [40]. In the simulations presented, this is satisfied and ion-ion correlations are negligible. The Rutherford differential scattering cross section gives a large-angle-only cross section of  $\sigma_L = \pi b_c^2$ . The probability of a large-angle collision in  $\Delta t$  is  $P_L = n v_{ij} \Delta t \pi b_c^2$ . The scattering probability density function given that a large-angle collision occurs is  $\mathcal{P}_L(\theta) d\theta = (1/\sigma_L)(d\sigma/d\theta) d\theta$ .  $C_L(\theta)$  is the cumulative distribution function defined by

$$C_L(\theta) = \int_{\theta_c}^{\theta} \mathcal{P}_L(\theta') d\theta' = -\frac{b_{\perp}^2}{b_c^2} \left[ \frac{1}{\sin^2(\frac{\theta'}{2})} \right]_{\theta_c}^{\theta}. \quad (6)$$

Using random numbers  $U \sim \mathcal{U}(0, 1)$  in the inverse cumulative distribution function,  $\theta = C_L^{-1}(U)$ , the large angles to perform scattering with are generated. The sign is positive or negative with equal probability. Note that  $C_L^{-1}(1) = \pi$  and  $C_L^{-1}(0) = \theta_c$ . Occasionally,  $P_L > 1$ , in which case  $\lfloor P_L \rfloor$  collisions are carried out with an extra collision if  $U < P_L - \lfloor P_L \rfloor$ .  $\lfloor P_L \rfloor$  is the floor function, which returns the largest integer not greater than  $P_L$ .  $U$  is not reused as at least one collision occurs if  $P_L > 1$ , and the random number comparison is with the noninteger portion of  $P_L$ , ensuring that the number of large-angle collisions is insensitive to  $\Delta t$ . This preserves the  $\mathcal{O}(N)$  operations scaling for  $N$  computational particles as the number of collisions of both types is  $(1 + P_L)N$ , with  $P_L$  independent of  $N$ .

Using this method, an ICF hot spot [41] is simulated. D, T, and electrons are initiated in thermal equilibrium at  $T = 5$  keV and  $n = 4.52 \times 10^{31} \text{ m}^{-3}$  in 0D3V. Figure 1 shows the yield for each of the three models for  $b_c$ , which

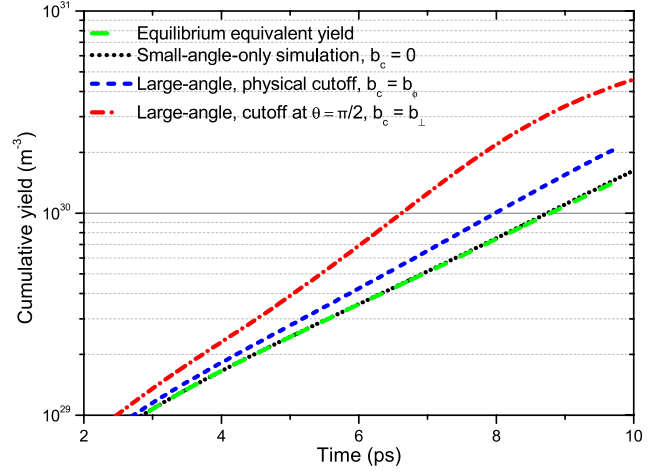


FIG. 1 (color online). Yield for ICF with a lossless hot spot using different values of the cutoff  $b_c$ .

begin to differ by  $t = 1.5$  ps. Both  $b_c = b_{\phi}$  and  $b_c = b_{\perp}$  show increases relative to  $b_c = 0$ . These are of 20% and 69%, respectively, at  $t = 6$  ps, compared to the burn time of 20–50 ps. The increase in yield feeds back into higher temperatures, and further reactions. The equilibrium equivalent yield is what would be expected for D and T in thermal equilibrium and having the  $b_c = 0$  temperature history. At the end of the simulations, the  $b_c = b_{\perp}$  model has a yield that is approximately 3 times higher than the small-angle-only  $b_c = 0$  simulation, while  $b_c = b_{\phi}$  gives a yield that is  $\sim 46\%$  higher. That the inclusion of large-angle collisions produces an increase in yield is a result which is not obvious given the reduction in energy loss via small-angle collisions that occurs because  $\ln \Lambda$  is replaced by  $\ln \Lambda_M$  when using  $b_c = b_{\perp}$  or  $b_c = b_{\phi}$ . Loss mechanisms, such as thermal conduction, radiation, and  $\alpha$  escape, are not included; even in this simple case, there is a significant discrepancy with small-angle-only theories. The less likely  $D + D$  and  $T + T$  fusion reactions are also omitted.

One possible explanation for the increased yield is the driving of non-Maxwellian distribution functions by large-angle collisions with  $\alpha$ s. These potentially enhance the tail of the distributions of D and T close to the peak of the fusion cross section. Figure 2 shows the distribution of  $\alpha$ s and D for the maximum departure from a Maxwellian. The D distribution is calculated time dependently and self-consistently; the athermal tail is driven by high energy  $\alpha$ s knocking thermal ions up to energies many times their initial energy. There is also thermal broadening of the  $\alpha$  distribution caused by high energy ions fusing. However, Fig. 2 shows the maximum departure from a Maxwellian in a reacting ion species for all simulations considered. D and T remain Maxwellian in the  $b_c = 0$ , small-angle-only simulation, while  $b_c = b_{\perp}$  only has small deviations from equilibrium, except for depletion effects at late times. But it is  $b_{\perp}$ , not  $b_{\phi}$ , which has the largest yield. Electrons

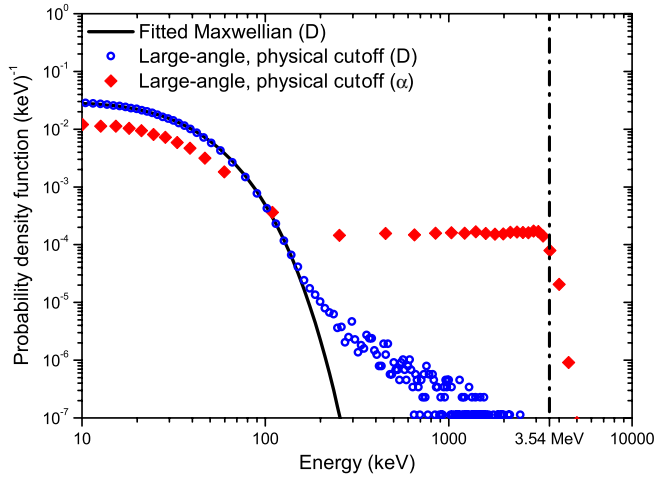


FIG. 2 (color online). Deuterium and  $\alpha$  distributions for  $b_c = b_\phi$  at the maximum departure of the D distribution from a Maxwellian as measured by the excess kurtosis,  $\kappa = \mu_4/\sigma^4 - 3$ .

always remain Maxwellian due to their short self-equilibration time. The athermal tail of the distribution formed for  $b_\phi$  is relatively small, as is the proportion of  $\alpha$  above their creation energy. Using the simulation data, time-integrated neutron spectra were obtained that showed no features attributable to the tail. The reason for the larger tail when using the  $b_c = b_\phi$  model is that  $b_\phi$  is larger than  $b_\perp$  for collisions between slowing  $\alpha$ s and fuel ions, so there are more knocked-on fuel ions relative to the other models.

The increases in yield for  $b_c \neq 0$  have another explanation. The increase is larger for  $b_\perp$  than for  $b_\phi$ , and it is found that  $b_\perp$  is greater for electron-ion collisions than  $b_\phi$ , whereas  $b_\phi$  is larger for ion-ion collisions. Therefore, fewer ions are knocked up to higher energies for  $b_\perp$ , but electrons absorb energy faster from  $\alpha$ s. With  $b_c = b_\perp$ , electrons also exchange energy faster with thermal ions, therefore increasing the equilibration rate and causing the ions to become hotter sooner. This is confirmed by smaller differences in temperature between fuel ions and electrons correlating with  $b_c \neq 0$ . The smallest  $\Delta T$  always occurs with  $b_c = b_\perp$ . This implies that a change in the rate of equilibration of temperature between electrons and ions causes the increase in yield.

To clearly demonstrate that higher ion temperatures occur earlier with large-angle collisions, we simulate equilibration without fusion. In Fig. 3, equilibration between D at  $T_D = 1$  keV and electrons at  $T_e = 0.5$  keV is shown, both with  $n = 2 \times 10^{30} \text{ m}^{-3}$ . Non-Maxwellians are not driven as the self-equilibration times of both species are shorter than their interspecies equilibration time. We compare equilibration using both the  $b_c = b_\phi$  and  $b = b_\perp$  models against the widely used Landau-Spitzer [5,29] small-angle equilibration model and its Monte Carlo equivalent  $b_c = 0$ . Both of these models use  $\ln \Lambda$  as defined below Eq. (4). In comparison to Landau-Spitzer or  $b_c = 0$  Monte Carlo calculations, large-angle collisions increase

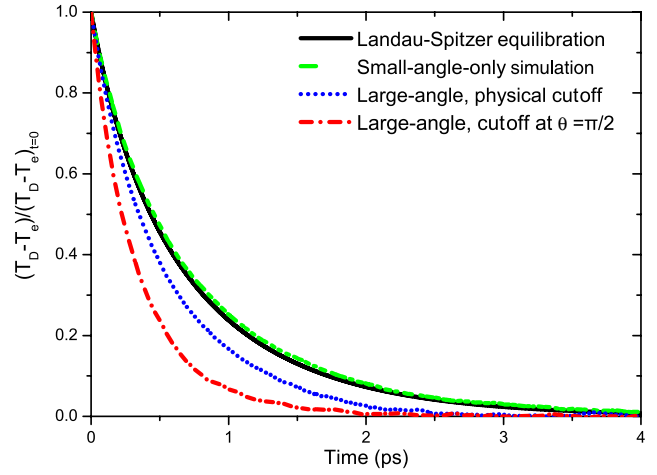


FIG. 3 (color online). Temperature equilibration rates comparing the Landau-Spitzer model, small-angle only ( $b_c = 0$ ), physically motivated cutoff ( $b_c = b_\phi$ ), and  $\theta = \pi/2$  ( $b_c = b_\perp$ ).

the equilibration rate. The rate increase is  $\sim 100\%$  for  $b_c = b_\perp$  and  $\sim 50\%$  for  $b_c = b_\phi$ . Therefore, the attainment of hotter ion temperatures earlier due to a higher electron-ion equilibration rate is the main cause of the increased yield in Fig. 1.

The effects on yield of considering thermal conduction, radiation, finite size, and large-angle collisions would require more detailed calculations. An indication that increased yield is likely in practice is obtained from the 1D radiation-hydrodynamics code NYM [42], which showed that a global increase of the electron-ion equilibration rate by 100% increased the yield of a 5 keV and  $\sim 140 \text{ g/cc}$  hot spot by 8% [43].

ICF experiments have not yet reached the conditions needed to ignite a hot spot. This is partly due to spatial hot spot nonuniformities [44]. The attainment of higher yields in the future will provide opportunities to verify the effects of large-angle collisions by comparing burn evolution with and without them within a more extensive model.

Additional effects such as particle indistinguishability, spin statistics, and nuclear elastic scattering (NES) are ignored. The equilibration rate increase identified in Fig. 3 is not affected by NES, which only acts between hadronic species. Though Coulomb and NES cross sections for ion-ion scattering at energies above 1 MeV are both of order barn [19,45], the cross sections (both small and large angle) for the stopping of fast ions on electrons by Coulomb collisions are much larger. Only for  $b_c = b_\perp$  and fast ion-ion scattering is the NES cross section greater than the large-angle collision cross section, implying that the most likely consequence of NES is a small enhancement of the tails on ion distributions. Also ignored are inelastic scattering processes and light nuclei break-up reactions [23].

The increase in electron-ion equilibration rate when including large-angle collisions is a surprising result given the corresponding reduction in the strength of small-angle

collisions, and is likely to be required to accurately calculate ICF yield. Large-angle collisions must be taken into account to obtain the correct temperature equilibration rate. The effects described cannot be predicted by fluid or VFP models, which are incapable of reproducing, self-consistently, the large jumps in particle energy that occur due to large-angle collisions.

We have provided a new technique to evaluate the effects of large-angle collisions in plasmas with  $\ln \Lambda \gtrsim 2$  and shown that their inclusion can have significant consequences for the yield in ICF due to an increased rate of temperature equilibration between ions and electrons.

A. E. T. is supported by an EPSRC Doctoral Prize Fellowship. The authors would like to thank Warren Garbett for helpful discussions.

---

\* a.turrell09@imperial.ac.uk

- [1] J. D. Lindl, *Phys. Plasmas* **2**, 3933 (1995).
- [2] J. Lindl, O. Landen, J. Edwards, E. Moses, and N. Team, *Phys. Plasmas* **21**, 020501 (2014).
- [3] K. A. Brueckner, H. Brysk, and R. S. Janda, *J. Plasma Phys.* **11**, 403 (1974).
- [4] M. J. Edwards *et al.*, *Phys. Plasmas* **18**, 051003 (2011).
- [5] B. A. Trubnikov, in *Reviews of Plasma Physics*, edited by M. A. Leontovich (Consultants Bureau, New York, 1965), Vol. 1, pp. 105–204.
- [6] R. S. Cohen, L. Spitzer, Jr., and P. McRoutly, *Phys. Rev.* **80**, 230 (1950).
- [7] D. V. Sivukhin, in *Reviews of Plasma Physics*, edited by M. A. Leontovich (Consultants Bureau, New York, 1966), Vol. 4.
- [8] C. P. Ridgers, C. S. Brady, R. Ducloux, J. G. Kirk, K. Bennett, T. D. Arber, A. P. L. Robinson, and A. R. Bell, *Phys. Rev. Lett.* **108**, 165006 (2012).
- [9] S. Son and N. Fisch, *Phys. Lett. A* **356**, 72 (2006).
- [10] J. P. Cox and R. T. Giuli, *Principles of Stellar Structure Volume II: Applications to Stars* (Gordon and Breach Science, New York, 1968).
- [11] S. J. Rose, *Astrophys. J. Lett.* **453**, L45 (1995).
- [12] H. Matsuura and Y. Nakao, *Phys. Plasmas* **13**, 062507 (2006).
- [13] D. Ryutov, *Phys. Scr.* **45**, 153 (1992).
- [14] M. Sherlock and S. J. Rose, *High Energy Density Phys.* **5**, 27 (2009).
- [15] D. Michta, F. Graziani, T. Luu, and J. Pruet, *Phys. Plasmas* **17**, 012707 (2010).
- [16] B. J. Albright, K. Molvig, C.-K. Huang, A. N. Simakov, E. S. Dodd, N. M. Hoffman, G. Kagan, and P. F. Schmit, *Phys. Plasmas* **20**, 122705 (2013).
- [17] K. Molvig, N. M. Hoffman, B. J. Albright, E. M. Nelson, and R. B. Webster, *Phys. Rev. Lett.* **109**, 095001 (2012).
- [18] G. Gorini, L. Ballabio, and J. Källne, *Rev. Sci. Instrum.* **66**, 936 (1995).
- [19] L. Ballabio, G. Gorini, and J. Källne, *Phys. Rev. E* **55**, 3358 (1997).
- [20] A. Andrade and G. M. Hale, *Phys. Rev. A* **30**, 1940 (1984).
- [21] J. Källne, L. Ballabio, J. Frenje, S. Conroy, G. Ericsson, M. Tardocchi, E. Traneus, and G. Gorini, *Phys. Rev. Lett.* **85**, 1246 (2000).
- [22] R. K. Fisher, P. B. Parks, J. M. McChesney, and M. N. Rosenbluth, *Nucl. Fusion* **34**, 1291 (1994).
- [23] J. A. Frenje *et al.*, *Nucl. Fusion* **53**, 043014 (2013).
- [24] F. Evans, *Phys. Fluids* **16**, 1011 (1973).
- [25] C.-K. Li and R. D. Petrasso, *Phys. Rev. Lett.* **70**, 3063 (1993).
- [26] X. Zha, S. Han, Z. Xu, and Y. Wang, *High Energy Density Phys.* **2**, 70 (2006).
- [27] Y. Afek, A. Dar, A. Peres, A. Ron, R. Shachar, and D. Shvarts, *J. Phys. D* **11**, 2171 (1978).
- [28] A. A. Korotkov, A. Gondhalekar, and R. J. Akers, *Phys. Plasmas* **7**, 957 (2000).
- [29] L. Spitzer, Jr., *Physics of Fully Ionised Gases* (Interscience, New York, 1967).
- [30] E. Greenspan and D. Shvarts, *Nucl. Fusion* **16**, 295 (1976).
- [31] S. T. Perkins and D. E. Cullen, *Nucl. Sci. Eng.* **77**, 20 (1981).
- [32] F. R. Graziani *et al.*, *High Energy Density Phys.* **8**, 105 (2012).
- [33] M. S. Murillo, *Phys. Plasmas* **11**, 2964 (2004).
- [34] N. David, Ph.D. thesis, Christ Church College, University of Oxford, 2005.
- [35] S. Chandrasekhar, *Rev. Mod. Phys.* **15**, 1 (1943).
- [36] D. Mihalas, *Stellar Atmospheres* (W. H. Freeman, San Francisco, 1939), 2nd ed., pp. 290–295.
- [37] T. Takizuka and H. Abe, *J. Comput. Phys.* **25**, 205 (1977).
- [38] A. E. Turrell, M. Sherlock, and S. J. Rose, *J. Comput. Phys.* **249**, 13 (2013).
- [39] B. Appelbe and J. Chittenden, *Plasma Phys. Controlled Fusion* **53**, 045002 (2011).
- [40] D. O. Gericke, M. S. Murillo, and M. Schlanges, *Phys. Rev. E* **65**, 036418 (2002).
- [41] O. L. Landen *et al.*, *Plasma Phys. Controlled Fusion* **54**, 124026 (2012).
- [42] P. D. Roberts, S. J. Rose, P. C. Thompson, and R. J. Wright, *J. Phys. D* **13**, 1957 (1980).
- [43] W. Garbett (private communication).
- [44] O. A. Hurricane *et al.*, *Nature (London)* **506**, 343 (2014).
- [45] J. A. Frenje, C. K. Li, F. H. Seguin, D. T. Casey, R. D. Petrasso, D. P. McNabb, P. Navratil, S. Quagliioni, T. C. Sangster, V. Y. Glebov, and D. D. Meyerhofer, *Phys. Rev. Lett.* **107**, 122502 (2011).